

Performance optimization of the neutron-sensitive image intensifier used in neutron imaging

Jinhao Tan(谭金昊), Yushou Song(宋玉收), Jianrong Zhou(周健荣), Wenqin Yang(杨文钦), Xingfen Jiang(蒋兴奋), Jie Liu(刘杰), Chaoyue Zhang(张超月), Xiaojuan Zhou(周晓娟), Yuanguang Xia(夏远光), Shulin Liu(刘术林), Baojun Yan(闫保军), Hui Liu(刘辉), Songlin Wang(王松林), Yubin Zhao(赵豫斌), Jian Zhuang(庄建), Zhijia Sun(孙志嘉), and Yuanbo Chen(陈元柏)

Citation: Chin. Phys. B, 2024, 33 (**8**): 086102. DOI: 10.1088/1674-1056/ad47ad

What follows is a list of articles you may be interested in

Silicon photomultiplier based scintillator thermal neutron detector for China Spallation Neutron Source (CSNS)

Xiu-Ping Yue(岳秀萍), Zhi-Fu Zhu(朱志甫), Bin Tang(唐彬), Chang Huang(黄畅), Qian Yu(于潜), Shao-Jia Chen(陈少佳), Xiu-Ku Wang(王修库), Hong Xu(许虹), Shi-Hui Zhou(周诗慧),Xiao-Jie Cai(蔡小杰), Hao Yang(杨浩), Zhi-Yong Wan(万志勇),Zhi-Jia Sun(孙志嘉), and Yun-Tao Liu(刘云涛)

Chin. Phys. B, 2023, 32 (**9**): 090402. DOI: 10.1088/1674-1056/ace316

A stopping layer concept to improve the spatial resolution of gas-electron-multiplier neutron detector

Jianjin Zhou(周建晋), Jianrong Zhou(周健荣), Xiaojuan Zhou(周晓娟), Lin Zhu(朱林), Jianqing Yang(杨建清), Guian Yang(杨桂安), Yi Zhang(张毅), Baowei Ding(丁宝卫), Bitao Hu(胡碧涛), Zhijia Sun(孙志嘉), Limin Duan(段利敏), and Yuanbo Chen(陈元柏)

Chin. Phys. B, 2022, 31 (**5**): 050702. DOI: 10.1088/1674-1056/ac398e

First neutron Bragg-edge imaging experimental results at CSNS

Jie Chen(陈洁), Zhijian Tan(谭志坚), Weiqiang Liu(刘玮强), Sihao Deng(邓司浩), Shengxiang Wang(王声翔), Liyi Wang(王立毅), Haibiao Zheng(郑海彪), Huaile Lu(卢怀乐), Feiran Shen(沈斐然), Jiazheng Hao(郝嘉政), Xiaojuan Zhou(周晓娟), Jianrong Zhou(周健荣), Zhijia Sun(孙志嘉), Lunhua He(何伦华), and Tianjiao Liang(梁天骄)

Chin. Phys. B, 2021, 30 (**9**): 096106. DOI: 10.1088/1674-1056/ac0da7

Performance optimization of the neutron-sensitive image intensifier used in neutron imaging

Jinhao Tan(谭金昊)[1,2,3], Yushou Song(宋玉收)[1,†], Jianrong Zhou(周健荣)[2,3,‡], Wenqin Yang(杨文钦)[2,3], Xingfen Jiang(蒋兴奋)[2,3], Jie Liu(刘杰)[1,2,3], Chaoyue Zhang(张超月)[1,2,3], Xiaojuan Zhou(周晓娟)[2,3], Yuanguang Xia(夏远光)[2,3], Shulin Liu(刘术林)[3], Baojun Yan(闫保军)[3], Hui Liu(刘辉)[4], Songlin Wang(王松林)[2,3], Yubin Zhao(赵豫斌)[2,3], Jian Zhuang(庄建)[2,3], Zhijia Sun(孙志嘉)[2,3], and Yuanbo Chen(陈元柏)[2,3]

[1] *Harbin Engineering University, Harbin* 150000, *China*

[2] *Spallation Neutron Source Science Center, Dongguan* 523803, *China*

[3] *State Key Laboratory of Particle Detection and Electronics, Institute of High Energy Physics, Chinese Academy of Sciences, Beijing* 100049, *China*

[4] *Key Laboratory of China Building Materials Industry for Special Photoelectric Materials, Institute of Special Glass Fiber and Optoelectronic Functional Materials, China Building Materials Academy, Beijing* 100024, *China*

(Received 27 January 2024; revised manuscript received 14 April 2024; accepted manuscript online 6 May 2024)

As a non-destructive testing technology, neutron imaging plays an important role in various fields, including material science, nuclear engineering, and fundamental science. An imaging detector with a neutron-sensitive image intensifier has been developed and demonstrated to achieve good spatial resolution and timing resolution. However, the influence of the working voltage on the performance of the neutron-sensitive imaging intensifier has not been studied. To optimize the performance of the neutron-sensitive image intensifier at different voltages, experiments have been performed at the China Spallation Neutron Source (CSNS) neutron beamline. The change in the light yield and imaging quality with different voltages has been acquired. It is shown that the image quality benefits from the high gain of the microchannel plate (MCP) and the high accelerating electric field between the MCP and the screen. Increasing the accelerating electric field is more effective than increasing the gain of MCPs for the improvement of the imaging quality. Increasing the total gain of the MCP stack can be realized more effectively by improving the gain of the standard MCP than that of the nMCP. These results offer a development direction for image intensifiers in the future.

Keywords: neutron detector, neutron imaging, microchannel plate, image intensifier

PACS: 61.05.Tv, 29.25.Dz, 29.40.Wk, 28.20.Pr **DOI:** 10.1088/1674-1056/ad47ad

1. Introduction

Due to the long penetration, isotope sensitivity, and other unique properties of neutrons, neutron imaging has become an invaluable tool in non-destructive fields. In recent years, based on the developments in neutron sources and neutron detection technology, advanced neutron imaging methods have been developed. For example, energy-resolved neutron imaging has advantages in the residual stress testing of industry materials and the component analysis of specific isotopes.[1,2] Phase-contrast neutron imaging improves imaging quality mainly by edge enhancement, which increases the visibility of sub-resolution structures and low-attenuation contrast materials.[3,4] Polarized neutron imaging provides the possibility to visualize magnetic fields.[5,6] Among all these neutron imaging methods, neutron detectors are crucial in determining the quality of neutron imaging.

A neutron detector composed of a neutron-sensitive scintillator, optical lens, and imaging camera is a widespread and cost-effective approach to achieving high imaging quality.[7–9] In such a detector, neutrons are converted into light by the scintillator, and then the light is focused on the camera to acquire images. To avoid neutron damage on the imaging chip, a reflecting mirror is also needed. In some experiments, an image intensifier must be employed to multiply the light emitted from the scintillator. For example, when performing energy-resolved neutron imaging, a time-stamping camera was used to collect the light emitted from the phosphor screen.[10] To reject the electronic noise, the pixels of the camera are difficult to trigger when the number of incident photons is less than 1000. An additional imaging intensifier is necessary in such a detector to ensure the light bright enough. A high-speed camera is appropriate to monitor the dynamic process of targets with high frame speeds. To acquire images with high signal-to-noise ratio, there must be enough light incident to a pixel in a single frame.[11] It is appropriate to use an image intensifier in such an imaging system. Moreover, for high-resolution imaging performed in low-flux neutron sources, the number of scintillation photons detected by the pixel may be insufficient due to the low neutron intensity.[12] The introduction of an image intensifier removes the photon statistics limitation.

Although the ability of light magnification provided by the image intensifier is necessary for these neutron imaging systems, the presence of an image intensifier also makes

†Corresponding author. E-mail: songyushou80@163.com

‡Corresponding author. E-mail: zhoujr@ihep.ac.cn

© 2024 Chinese Physical Society and IOP Publishing Ltd

the imaging system complex. In our previous work, a neutron-sensitive image intensifier was developed by coupling a neutron-sensitive microchannel plate (nMCP), a standard microchannel plate (MCP), and a phosphor screen.[13] In such a device, the process of neutron conversion and light magnification can be realized, which helps to decrease the complexity of the imaging system. It not only meets the demands of specific neutron imaging experiments, such as energy-resolved neutron imaging and high-resolution imaging in low-flux neutron sources, but can also be used in normal neutron imaging experiments. Comparing with the combination of a phosphor screen and a standard image intensifier, there are some advantages for neutron-sensitive image intensifier. The normal image intensifier is sensitive to the environment photons because of the high quantum efficiency of the photocathode. This means that even a single photon from the environment incident to the image intensifier contributes to the noise of the imaging result. As a result, an imaging system equipped with a normal image intensifier needs strict protection from the light. With regard to the neutron-sensitive imaging intensifier, it has almost no sensitivity to the ambient light; therefore, it is almost free from protection from the light. In addition, with the combination of the phosphor screen and standard image intensifier, the clusters triggered by the neutron events are multiple separated points.[14] With a neutron-sensitive image intensifier, the clusters triggered by neutrons are spatially continuous.[13] This means that analyzing the neutron events in a neutron image intensifier is easier and clearer than that in a standard image intensifier.

China Spallation Neutron Source (CSNS) is the fourth high-flux pulsed spallation neutron source facility in the world.[15] At CSNS, an energy-resolved neutron imaging instrument has been established. A neutron detector based on a neutron-sensitive image intensifier coupled with a time-stamping camera is one of the candidates for the imaging detector for this instrument. In our previous study, we showed that 25 μm spatial resolution can be achieved and a preliminary energy-resolved neutron imaging experiment was performed using such a detector. However, as a crucial device for the detector, the performance of the neutron-sensitive image intensifier has not been optimized. The working voltage is an important parameter to determine the gain of the neutron-sensitive image intensifier. The electron drift process is also influenced by the voltages, which are related to the image quality. In this paper, the change in the light yield and the image quality with the working voltage were studied. A conventional neutron imaging experiment was conducted by coupling with a camera. The results of this paper will guide the development of the neutron-sensitive image intensifier in the future.

2. Design of the neutron-sensitive image intensifier

The structure of the neutron-sensitive image intensifier is shown in Fig. 1(a). It includes a neutron-sensitive microchannel plate, a standard MCP, and a phosphor screen. The nMCP and the standard MCP were manufactured by the China Building Materials Academy and sealed as a neutron-sensitive image intensifier by Northern Night Vision. Ltd. The nMCP is the key component of the neutron-sensitive image intensifier, which determines the performance quality, such as detection efficiency and spatial resolution. In this work, the nMCP is doped with 20 mol% $^{10}B_2O_3$ with 8 μm pore diameter, 10 μm pitch, and 3° bias angle. According to the calculation, 36% detection efficiency of thermal neutrons could be achieved. Compared with the Gd-doped nMCP in other institutes, the boron-doped nMCP provides better neutron–gamma discrimination capability and spatial resolution. Meanwhile, the gain of the nMCP was suppressed to a low level during manufacturing to further improve the neutron–gamma discrimination capability.[16] A standard MCP with 10 μm pore diameter, 12 μm pitch, and 12° bias angle was followed with the nMCP to decrease the ion feedback effect and increase the total gain of the neutron-sensitive image intensifier. The nMCP and the standard MCP were spaced by a 0.1 mm thickness electrode. The electron clouds converted by neutron events were then collected by the phosphor screen. With regard to the phosphor screen, the influence of the light yield, emission spectrum, and decay time should be considered. The material of the phosphor screen determines the time properties of the neutron-sensitive image intensifier. In this study, $Y_3Al_5O_{12}$:Ce (P46) was selected. It has a fast decay time and relatively high light yield. The peak of the light spectrum is about 530 nm, which is located in the high quantum efficiency range of typical image sensors. The P46 phosphor screen can be replaced by P47 when the timing resolution is the most concerning performance. Figure 1(b) shows a photograph of the neutron-sensitive image intensifier. It is a portable device of about 65 mm diameter.

To study the performance of the neutron image intensifier under different working voltages, a voltage divider was also designed. The MCPs can be regarded as the paralleling resistance and capacitance in a circuit. When providing a high voltage to an MCP electrode directly, the potential of other electrodes is also influenced. To overcome this problem, a voltage divider was designed, as shown in Fig. 2. To ensure that each channel of the power supply operates normally, the output current of each channel should be positive. In this study, the resistance of the nMCP is 2200 MΩ, and that of the standard MCP is 113 MΩ (at 500 V). The resistance of R_1, R_2, and R_3 is 10 MΩ, 10 MΩ, and 2 MΩ, respectively; R_{11}, R_{22}, and R_{33} are all 100 kΩ.

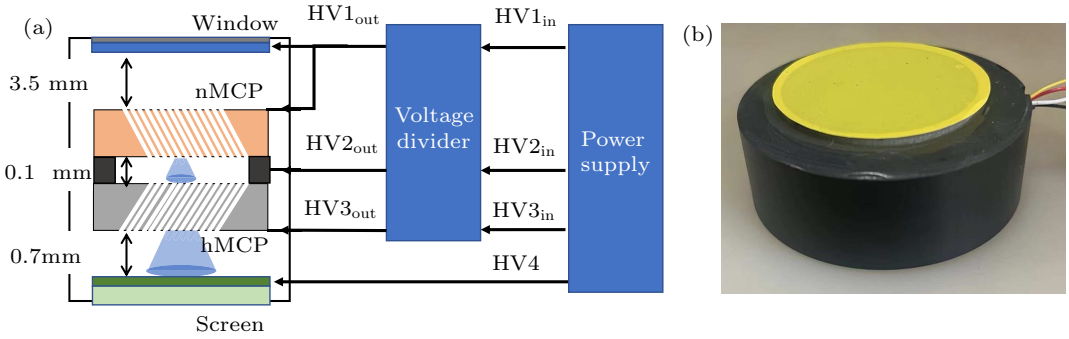


Fig. 1. (a) A diagram of the neutron-sensitive image intensifier. (b) A photograph of the neutron-sensitive image intensifier.

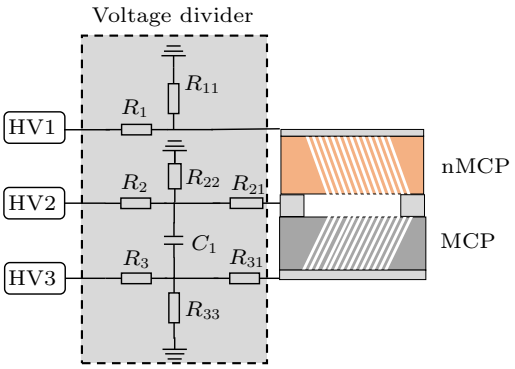


Fig. 2. A diagram of the voltage divider.

3. Results and discussion

3.1. The relative light output at different voltages

Light output is one of the crucial parameters of the image intensifier, which influences the signal-to-noise ratio and the contrast ratio of the imaging results. It is important to study the changes in the light output with the voltages of the neutron-sensitive image intensifier.

In the field of neutron detection, the light output is commonly defined as the number of photons generated by neutron absorption. Many methods of light output measurement have been developed in previous studies, such as the pulse method, a method based on the measurement of the intrinsic resolution of the photomultiplier, a single-electron method, and the comparison method.[17] An experiment based on the comparison method was conducted at CSNS beamline 20. The comparison method, which is based on the comparison of light intensity from the tested detector and the reference detector with a certain light intensity, is convenient for measuring the relative high light output of the detector. To study the change in the light output with the voltages, we take the light output of the neutron-sensitive image intensifier under certain conditions as the reference in this experiment. In this way, the difference in the response efficiency (for the neutron beam and the accompanying gamma rays) between the reference detector and test detector can be eliminated. A diagram of the experiment is shown in Fig. 3(a). A neutron imaging detector was prepared using a neutron-sensitive image intensifier, a reflecting mirror, an optical lens, and a CMOS camera (PCO edge 4.2). Non-linearity less than 0.5% can be achieved by the CMOS camera used in this experiment, which means the relationship between the grayscale and the light intensity can be regarded as linear. The diameter of the neutron beam was limited to 10 mm diameter to avoid overexposure.

Figure 3(c) shows a typical imaging result from the neutron beam acquired by the neutron-sensitive image intensifier. The bright circle in Fig. 3(c) corresponds to the region irradiated by the neutron beam. The larger dark circle in Fig. 3(c) corresponds to the whole effective area of the neutron-sensitive image intensifier. The light intensity in this region is mainly contributed by the dark counts for the MCPs, which is largely lower than that of the neutron beam region. The spectrum corresponding to Fig. 3(c) is shown in Fig. 3(d). It can be divided into a peak contributed by the bright neutron beam, and a continuous spectrum contributed by the dark counts. In this experiment, the light output and the dark counts for different conditions were quantitatively calculated from the mean of the peak and that of the continuous spectrum, respectively. To avoid overexposure of the imaging sensor, the grayscale in this experiment is controlled below 65536 by limiting the voltage of the neutron-sensitive image intensifier. We did not study the maximum light output of the neutron-sensitive image intensifier, but the trend of the light output changed with the voltages.

The neutron-sensitive image intensifier is influenced by the gain of MCPs and the properties of the P46 screen. The light output can be acquired by adjusting the voltages of the nMCP (represented as V_1), the standard MCP (represented as V_2), and the space between the MCP and the screen (represented as V_3). During the experiment, V_1, V_2, and V_3 were changed dividedly: V_1 was changed from 600 V to 950 V, where V_2 was 950 V and V_3 was 3000 V; V_2 was changed from 800 V to 1150 V, where V_1 was 750 V and V_3 was 3000 V; and V_3 was changed from 2500 V to 4600 V, where V_1 was 750 V and V_2 was 950 V. Each condition was measured for 10 frames, and each frame was exposed for 5 s.

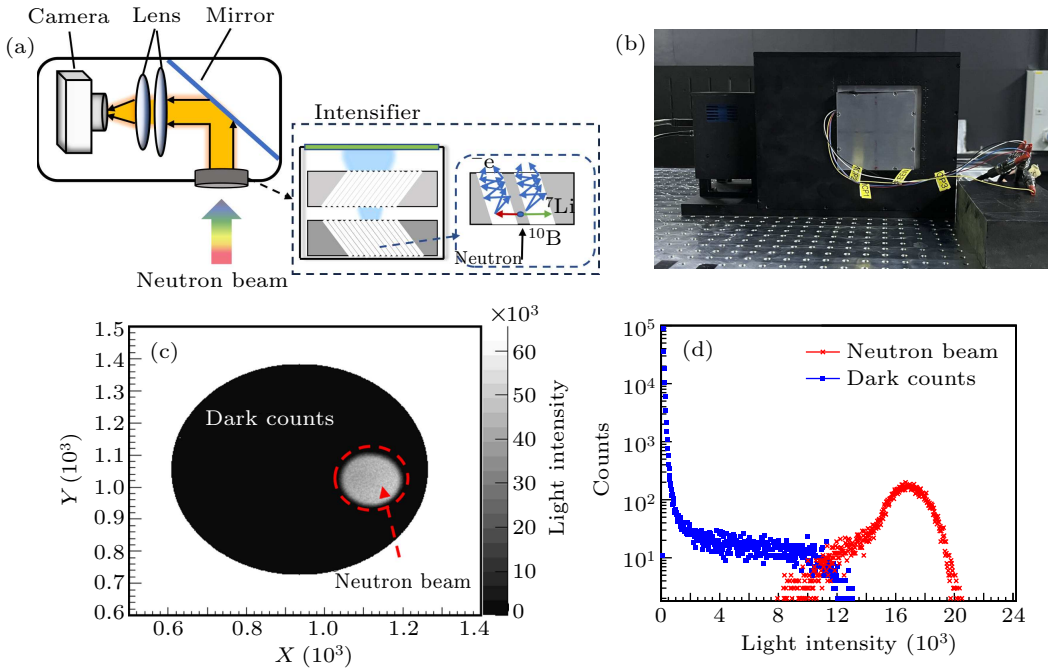


Fig. 3. (a) A diagram of the experimental setup for the light output measurement. (b) A photograph of the experimental detector. (c) A typical imaging result for the neutron beam acquired by the neutron-sensitive image intensifier. (d) A typical light intensity spectrum of the neutron-sensitive image intensifier.

The light output for V_1 at 750 V, V_2 at 800 V, and V_3 at 3000 V was taken as the reference condition. Then, the relative light output can be calculated according to

$$Y_{\rm r} = \frac{Y_{\rm NII} - Y_{\rm D1}}{Y_{\rm Ref} - Y_{\rm D2}}, \tag{1}$$

where $Y_{\rm r}$ is the relative light output, and $Y_{\rm NII}$ and $Y_{\rm Ref}$ are the light intensity of the tested conditions and the reference conditions of the neutron-sensitive image intensifier, respectively. Here, $Y_{\rm D1}$ and $Y_{\rm D2}$ are the backgrounds contributed by the dark counts for the tested conditions and the reference conditions. Using Eq. (1), the variation of $Y_{\rm r}$ with V_1, V_2, and V_3 was calculated and is presented in Fig. 4. Obviously, the relative light output increases with the increase in the voltages of nMCP (V_1) and MCP (V_2). In Fig. 4(a), it is found that the speed of increase in $Y_{\rm r}$ is faster at the higher V_1 and V_2, which is consistent with the gain curve for the MCPs.[18] This is due to the increasing secondary electron yield for MCPs with the higher secondary electron energy in the channels. Besides the improvement in the MCP voltages, V_2 results in a higher increase in the relative light yield $Y_{\rm r}$ when compared to the improvement in the nMCP voltage by V_1. This is due to higher electron multiplication gain in the standard MCP than that in the nMCP. With the nMCP, the neutrons can be absorbed anywhere in the nMCP substrate. The gains of the electron multiplication for the deeply absorbed neutron are less than those of neutrons absorbed at the top of the substrate. This decreases the average electron multiplication gains for the nMCP. With the standard MCP, most electrons initiate electron avalanches at the MCP surface. The electron multiplication gain for the standard MCP is more than that for the nMCP, which means the total gain of the MCPs can be improved more effectively by increasing the secondary electron yield of the standard MCP.

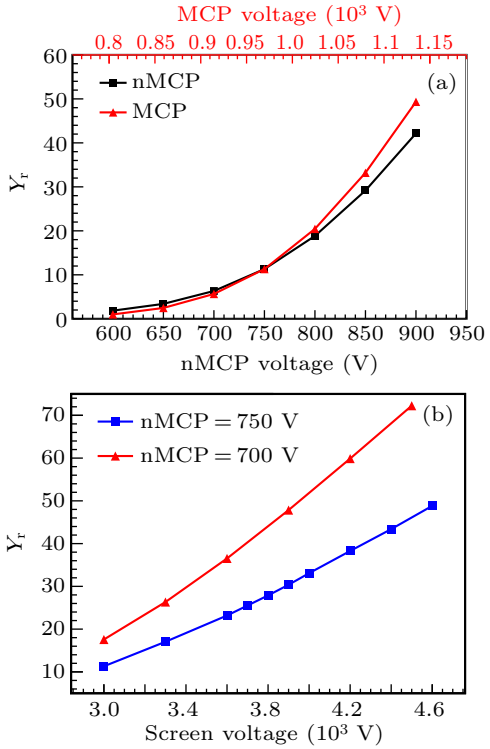


Fig. 4. (a) Curves of the relative light yield with different nMCP (V_1) and MCP (V_2) voltages. (b) Curves of the relative light yield with different screen (V_3) voltages.

Figure 4(b) shows that the curves of the relative light yield $Y_{\rm r}$ changed with the V_3 voltages. In contrast with the trend in Fig. 3(a), the light yield increases linearly with the V_3 voltages. This reflects the relationship between the energy of the accelerated electrons and the deposition energy of these electrons

on the screen. Moreover, because of the presence of residual gas between the standard MCP and the screen, more electrons reach the screen with the increase in the accelerating electric field, which also contributes to this trend. According to Fig. 4, the relative light yield of the neutron-sensitive image intensifier improves about 72 times compared with the reference conditions. The error of this measurement is only contributed by the fluctuation of the neutron flux. Due to the stability of the accelerator, the neutron beam fluctuation is evaluated at about 1%. In the future, an experiment to measure the absolute light output of the neutron image intensifier will be conducted.

3.2. Imaging quality with different voltages

Imaging quality is the key performance for the final imaging results. Using a commercial test target (such as the USAF target[19] and the Siemens-star target[13]), the quantitative spatial resolution can be acquired by analyzing the line pair in the images. However, the analysis of the spatial resolution via this method requires the data statistics to be high enough. It is not an appropriate method when a series of conditions need to be tested because of the high cost of beam time. Besides, the imaging quality can also be estimated by imaging using a specific knife or step-edge pattern.[20,21] The point spread function (PSF) can be derived according to the knife or step-edge image. The spatial resolution of the imaging system can be determined using these methods, but a specific target should be prepared. For the experiments without a target, it would be interesting if the image quality could be analyzed based on the inherent pattern of the imaging system. In this experiment, we try to compare the imaging quality under different voltages based on a small crack on the MCPs. Among the millions of channels of the MCP, there are always some broken channels, resulting in no gain in the corresponding region and shown as a dark spot in the imaging results (Fig. 5(d)). In the region with no gain, there are still photons that are spread from the surrounding region registered by the image sensor. In the imaging results, the relationship between the grayscale distribution in the dark spot and the image quality is discussed first.

Assuming that a system has unit magnification, the object irradiance distribution of a surface light source with a dark spot $f(x,y)$ can be described by

$$f(x,y)=\begin{cases}1, & (\sqrt{x^2+y^2}>r_0),\\ 0, & (\sqrt{x^2+y^2}<r_0),\end{cases} \tag{2}$$

where r_0 is the radius of the dark spot. When the light goes through the imaging system, the light spreads and results in the image blurring. The response in the image plane $g(x,y)$ can be calculated using the convolution of the $f(x,y)$ and PSF(x,y), where PSF(x,y) is the point spread function of the imaging system. Typically, the PSF(x,y) is assumed to be a two-dimensional Gaussian function with the standard deviation $\sigma_{\rm PSF}$. Then, the $g(x,y)$ in such conditions can be calculated by breaking the continuous response into a set of point sources at specific locations, each with a PSF(x,y) at a particular location, as shown in Fig. 5(a). The response in the cracked region is contributed by the spread of light from the surrounding area. Then, by projecting the $g(x,y)$ to the X axis and fitting the projected curve using a Gaussian function, as shown in Fig. 5(b), the standard deviation of the fitted curve $\sigma_{\rm Fit}$ can be acquired. It is found that $\sigma_{\rm fit}$ is proportional to the standard deviation of the PSF function $\sigma_{\rm PSF}$. This implies that the image quality can be evaluated according to the $\sigma_{\rm fit}$. Although the quantitative resolution cannot be acquired via this method, it is convenient to compare the imaging quality in different parameters and thus contribute to the optimization of the neutron-sensitive image intensifier.

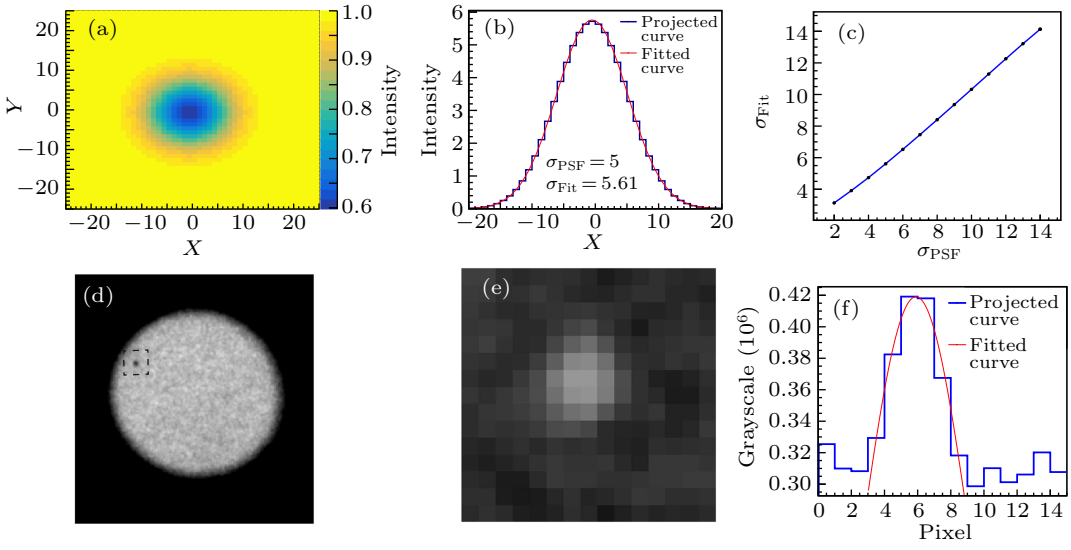


Fig. 5. (a) A diagram of the image response for a surface light source with a dark spot. (b) The projected curve of the image irradiance distribution $g(x,y)$. (c) The relationship of $\sigma_{\rm PSF}$ and the standard deviation of the grayscale in the dark spot $\sigma_{\rm Fit}$. (d) A typical neutron beam imaging result acquired by the neutron-sensitive image intensifier. (e) A zoomed image of the dark spot in (d). (f) The projected curve for (e).

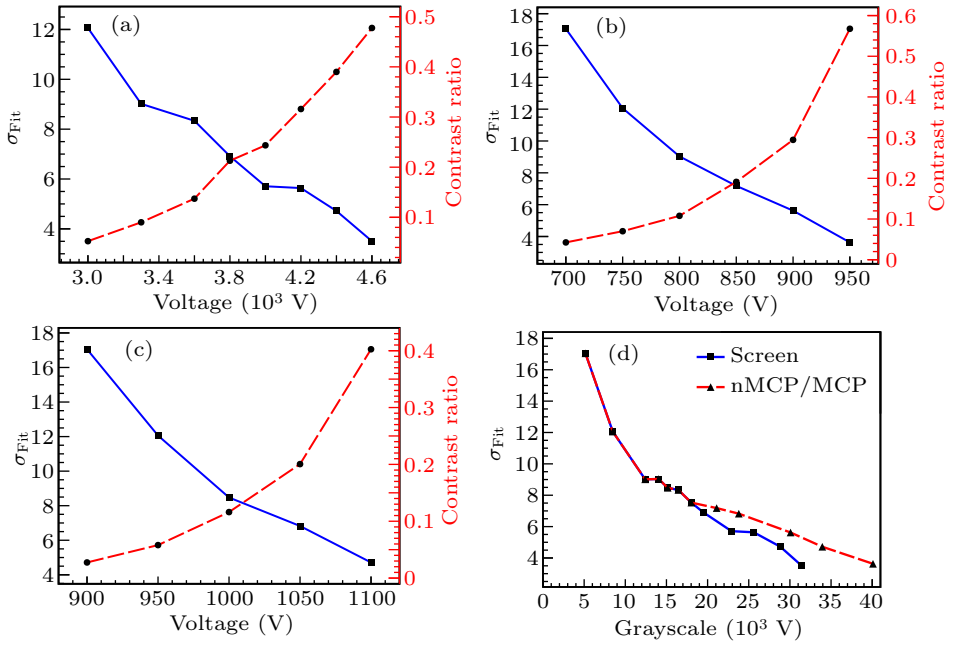


Fig. 6. (a) The changes in σ_f and the contrast ratio with the voltages in the nMCP V_1, where the voltage for the standard MCP V_2 is 950 V and the voltage between the standard MCP and the screen V_3 is 3000 V. (b) The changes in σ_f and the contrast ratio with the voltages in the standard MCP V_2, where V_1 is 750 V and V_3 is 3000 V. (c) The changes in σ_f and the contrast ratio with V_3, where V_1 is 750 V and V_2 is 950 V.

Figure 5(d) shows an image of the 10 mm diameter neutron beam acquired by the neutron-sensitive image intensifier. A dark spot caused by the MCP's cracked channels can be seen. For convenience, the grayscale of each pixel in Fig. 5(d) $g_0(x,y)$ was converted to $g_1(x,y)$ using

$$g_1(x,y) = 65535 - g_0(x,y), \tag{3}$$

where 65535 is the maximum grayscale of a pixel for the image sensor. The converted image is shown in Fig. 5(e). Then, the σ_{fit} is acquired by projecting the image in Fig. 5(e) to the X-axis and fitting the peak using a Gaussian function, as shown in Fig. 5(f).

The changes in the curves of σ_f with the voltages for V_1, V_2, and V_3 are shown in Fig. 6. According to the results in Figs. 6(a) and 6(b), the image quality is improved with the increase in the voltages of the MCPs. For the nMCP and MCP, the increase in the voltages results in an improvement in the gain and photon emission from the screen. The contrast ratio can be improved with such a process and better imaging quality is achieved. The contrast ratio can be calculated according to

$$\text{Contrast ratio} = \frac{I_{max} - I_{min}}{I_{max} + I_{min}}, \tag{4}$$

where I_{max} is the maximum grayscale and I_{min} is the minimum grayscale in the imaging result. The change in the contrast ratio with voltages is also shown as the dashed line in Fig. 6. In Fig. 6(c), the imaging quality also improves with the higher V_3 voltages. With regard to the screen, the contrast ratio can also be improved by increasing the voltage between the MCP and the screen. Besides, the stronger accelerating electric field limits the spread of electrons during the transport between the standard MCP and the screen. This means smaller light spots can be acquired under the higher voltage.

According to Figs. 6(a)–6(c), the imaging quality varies monotonically with the working voltages, which is similar to the trend of the light yield. To understand the relationship between the light yield and the image quality, curves of the light yield and the image quality were acquired, as shown in Fig. 6(d). There are two curves seen in Fig. 6(d). When the grayscale is higher than 18000, the curve with a smaller σ_{fit} corresponds to the change in V_3. It implies that the imaging quality can be improved more effectively by increasing V_3 than by increasing V_1 and V_2. With regard to the MCPs, no difference was found between increasing the gain of the nMCP and that of the standard MCP in improving the imaging quality.

Evaluation of the resolution using the "dark spot" method is not a traditional method. To demonstrate the results acquired via the "dark spot" method in another way, imaging results for the Siemens-star target under different screen voltages were acquired. The screen voltages were changed from 3800 V to 3000 V. Each condition was measured for 5 minutes. The imaging results for 3800 V, 3600 V, 3200 V, and 3000 V are shown in Figs. 7(a), 7(b), 7(c) and 7(d), respectively. The grayscale in each image was adjusted into the same range. The imaging result with higher voltage is brighter than that with a lower voltage. Based on the edge between two lines in Fig. 7(a) (in the square), the line spread function (LSF) for each image was acquired, as shown in Fig. 7(e). The full width at half maximum (FWHM) for the LSF of the lower screen voltage is wider than that of the higher voltage.

This implies that a better contrast ratio can be achieved using a higher screen voltage, which is consistent with the conclusion acquired by Fig. 6. The changes in resolution between different voltage conditions are not obvious, because the statistics in the imaging results are not enough.

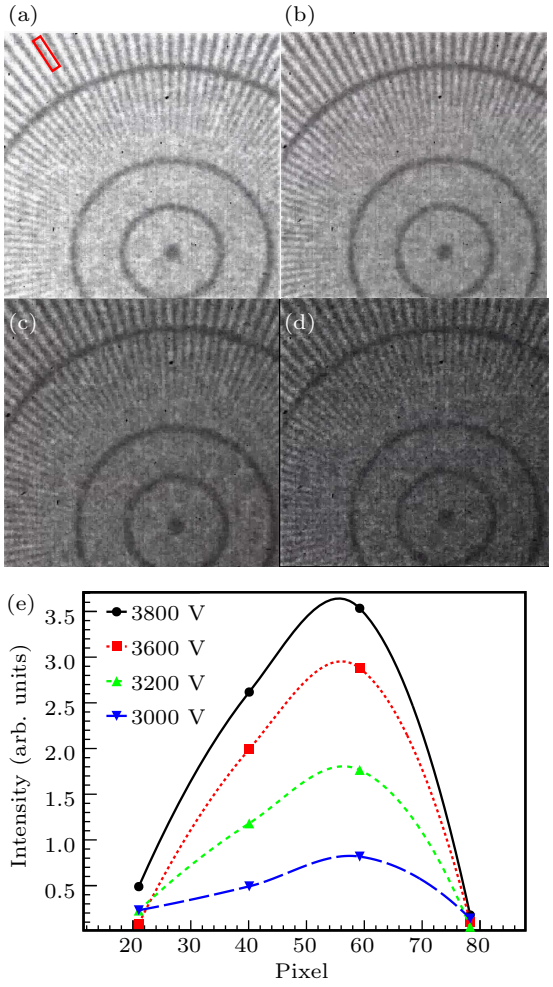


Fig. 7. The imaging results of the Siemens-star target with the screen voltages at (a) 3800 V, (b) 3600 V, (c) 3200 V, and (d) 3000 V. (e) The LSF curves for the imaging results with different screen voltages.

According to the results in Fig. 4(a), the total gain of the MCPs can be increased more effectively by increasing the gain of the standard MCP. Meanwhile, it has been demonstrated that an nMCP with low gain benefits the neutron–gamma discrimination.[16] Therefore, coupling an nMCP with relatively low gain and a standard MCP with high gain achieves good performances. Development of the materials and method to improve the secondary electron yield of the MCP channel surface will be a good way to improve the MCP gain.

3.3. Neutron imaging experiment with the neutron-sensitive image intensifier

To validate the imaging ability of the neutron-sensitive image intensifier, a neutron imaging experiment with the Siemens-star target was performed by coupling a conventional CCD camera (Princeton Instruments, SOPHIA 2048B) with 2048×2048 pixels and 15 μm pixel size. The voltages of the neutron-sensitive image intensifier were 750 V for V_1, 950 V for V_2, and 3800 V for V_3. The optical magnification for the optical lens was 0.3. The imaging results for the Siemens-star target were exposed for 50 minutes and then divided by an open beam image to eliminate the beam nonuniformity, as shown in Fig. 8(a). To quantitatively estimate the resolution, the modulation transfer function (MTF) curve of Fig. 8(a) was calculated, as shown in Fig. 8(b). Typically, the spatial resolution can be represented by the MTF at 0.1. In this result, the spatial resolution is about 7 lp/mm, which corresponds to 71 μm per line pair.

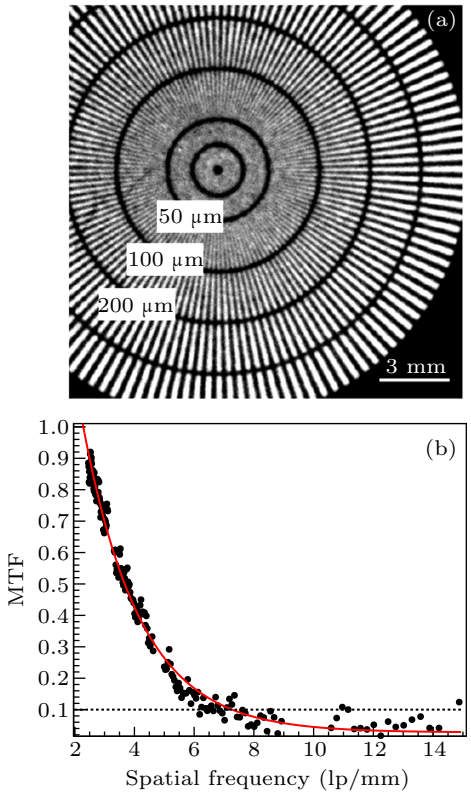


Fig. 8. (a) The neutron imaging for the Siemens-star target. (b) The MTF curve.

In our previous studies, the neutron-sensitive image intensifier was used to perform energy-resolved neutron imaging with spatial resolution for about 100 μm per line pair by coupling a time-stamping camera with 55 μm×55 μm pixel size and implementing a centroiding algorithm.[13] The spatial resolution can be improved by decreasing the optical magnification with the decrease in the field-of-view (FOV). Compared with the imaging results of this experiment, better spatial resolution was achieved with the same optical magnification and smaller pixel size, even though no reconstruction process was performed. This demonstrates that higher resolution neutron imaging can be easily performed by the neutron-sensitive image intensifier by coupling to a camera with smaller pixel size. To further improve the spatial resolution of the neutron-sensitive image intensifier, the size of the electron cloud emitted by the nMCP and standard MCP should be decreased by

optimizing the structure of the neutron-sensitive image intensifier. For example, the distance between the standard MCP and the screen can be decreased (0.7 mm currently). Besides, an additional electric field can be implemented between the nMCP and standard MCP to limit the electron diffusion between the gap. Ideally, spatial resolution better than 20 μm can be achieved using the neutron image intensifier, which is limited by the channel diameter and the range of products generated by neutron absorption. With the ability of high light yield and high resolution, the neutron-sensitive image intensifier will be a competitive device in various neutron imaging applications, such as energy-resolved neutron imaging and high-resolution neutron imaging.

4. Conclusion and outlook

The performances of the neutron-sensitive image intensifier changing with the working voltages were studied in this study. It is shown that the light yield and the imaging quality both benefited from the increase in the gain of MCPs and the electric field between the standard MCP and the screen. For the MCPs, the imaging quality is improved due to the higher contrast ratio under the higher MCP gain. The total gain of the MCPs can be improved more effectively by increasing the secondary yield of the standard MCP. With regard to the screen, the increase in the electric field between the standard MCP and the screen not only improves the contrast ratio of the images but also limits the spread of the electron cloud. This is why improving the electric field between the standard MCP and the screen is more effective in improving the imaging quality than increasing the gain of MCPs. These results provide a direction to optimize the parameters of the neutron image intensifier in the future. Moreover, the neutron imaging experiments also demonstrate that, as well as conducting energy-resolved neutron imaging by coupling with a time-stamping camera, the neutron-sensitive image intensifier can also be used for high-resolution neutron imaging by coupling with a camera with small pixel size.

In the future, the neutron-sensitive image intensifier with a relatively low-gain nMCP, a high-gain standard MCP, and a large sensitive area of about 100 mm diameter will be manufactured. The structure of the image intensifier will be optimized to further decrease the electron cloud size and improve the spatial resolution. We believe that it will be a competitive device in the neutron imaging field because of its high imaging quality and light yield.

Acknowledgements

Project supported by the National Key R&D Program of China (Grant Nos. 2023YFC2206502 and 2021YFA1600703), the National Natural Science Foundation of China (Grant Nos. 12175254 and 12227810), and the Guangdong–HongKong–Macao Joint Laboratory for Neutron Scattering Science and Technology.

References

[1] Su Y H, Kenichi O, Takenao S, Tetsuya K, Takashi H, Osamu I, Yoshitaka M and Yo T 2021 *Sci. Rep.* **11** 4155
[2] Anton S T, John R, Takenao S, Winfried K, Adrian S L and Sven C V 2017 *Sci. Rep.* **7** 40759
[3] Allman B E, McMahon P J, Nugent K A, Paganin D, Jacobson D L, Arif M and Werner S A 2000 *Nature* **408** 158
[4] Strobl M, Treimer W, Kardjilov N, Hilger A and Zabler S 2008 *Nucl. Instrum. Methods Phys. Res. A* **266** 181
[5] Jacopo V, Ralph P H, Marc R, Muriel D S, Manuel M, Pierre B, Markus S, Patrick H, Lothar H, Uwe F, Wolfgang T, Florian M P and Christian G 2019 *Nat. Commun.* **10** 3788
[6] Manke I, Kardjilov N, Schäfer R, Hilger A, Grothausmann R, Strobl M, Dawson M, Grünzweig C, Tötzke C, David C, Kupsch A, Lange A, Hentschel M P and Banhart J 2015 *Phys. Procedia* **69** 404
[7] Jiang X F, Xiu Q L, Zhou J R, Yang J Q, Tan J H, Yang W Q, Zhang L J, Xia Y G, Zhou X J, Zhou J J, Zhu L, Teng H Y, Yang G A, Song Y S, Sun Z J and Chen Y B 2021 *Nucl. Eng. Technol.* **53** 1942
[8] Daniel S H, Jacob M L, Elias B and David L J 2017 *Nucl. Instrum. Methods Phys. Res. A* **866** 9
[9] Pavel T and Eberhard H L 2016 *J. Phys.: Conf. Ser.* **746** 012004
[10] Yang J Q, Zhou J R, Jiang X F, Tan J H, Zhang L J, Zhou J J, Zhou X J, Yang W Q, Xia Y G, Chen J, Sun X L, Zhang Q H, Li J, Sun Z J and Chen Y B 2021 *Nucl. Instrum. Methods Phys. Res. A* **1000** 165222
[11] Segawa M, Kai T, Sakai T, Ooi M and Kureta M 2013 *Nucl. Instrum. Methods Phys. Res. A* **697** 77
[12] Mizutani R, Abe Y, Arikawa Y, Nishibata J, Yogo A, Mirfayzi S R, Nishimura H, Mima K, Fujioka S, Nakai M, Shiraga H and Kodama R 2020 *High Energy Density Phys.* **36** 100833
[13] Tan J H, Song Y S, Zhou J R, Yang W Q, Jiang X F, Zhou X J, Xia Y G, Liu S L, Yan B J, Liu H, Wang S L, Sun Z J, Wei Y D and Chen Y B 2024 *JINST* **19** P01015
[14] Losko A S, Han Y, Schillinger B, Tartaglione A, Morgano M, Strobl M, Long J, Tremsin A S and Schulz M 2021 *Sci. Rep.* **11** 21360
[15] Wei J, Chen H S and Chen Y W, *et. al.* 2009 *Nucl. Instrum. Methods Phys. Res. A* **600** 10
[16] Tan J H, Song Y S, Zhou J R, Zhou J J, Jiang X F, Zhou X J, Yang W Q, Xia Y G, Liu S L, Yan B J, Liu H, Wang S L, Sun Z J and Chen Y B 2023 *Nucl. Instrum. Methods Phys. Res. A* **1047** 167828
[17] Sysoeva E, Tarasov V and Zelenskaya O 2002 *Nucl. Instrum. Methods Phys. Res. A* **486** 67
[18] Xu Y L, Xu T, Liu H, Cai H and Wang C L 2017 *Int. J. Mass Spectrom.* **421** 234
[19] Finocchiaro V, Aliotta F, Tresoldi D, Ponterio R C, Vasi C S and Salvato G 2013 *Rev. Sci. Instrum.* **84** 093701
[20] Yang T, Zhou J R, Zhou X J, Zhu L, Zhu H Y, Zhou J J, Xia Y G, Wei Y D, Jiang X F, Yang W Q, Yang G A, Wang S L, Xie Y G, Sun Z J, Ouyang Q, Zhu J T, and Chen Y B 2022 *IEEE Trans. Nucl. Sci.* **69** 68
[21] Zhou J J, Zhou J R, Zhou X J, Zhu L, Yang W Q, Xu H, Guan B J, Wang S L, Yang J Q, Yang G A, Xie Y G, Zhang Y, Ding B W, Hu B T, Sun Z J, Duan L M and Chen Y B 2022 *Nucl. Instrum. Methods Phys. Res. A* **1024** 166076